Received: 20 November 2023 | Revised: 15 March 2024 | Accepted: 15 March 2024

DOI: 10.1002/suco.202301005

ARTICLE

fib CEB-FIP WILEY

The Wieselburg Bridge collapse—Analysis of the shear capacity based on forensic data

Tobias Huber | **Johann Kollegger** | **Dominik Suza** | **Patrick Huber**

Institute for Structural Engineering, Vienna University of Technology, Vienna, Austria

Correspondence
Tobias Huber, Institute for Structural Engineering, Vienna University of Technology, Karlsplatz 13/212-2, 1040 Vienna, Austria.
Email: tobias.alexander.huber@tuwien.ac.at

Abstract

This paper describes the structural aspects of the Wieselburg Bridge collapse in Austria. The original design and reinforcing details for this integral concrete bridge are discussed. The collapse of the bridge is re-constructed based on forensic documentation of the failure. The results of structural analysis carried out using material properties obtained after failure are compared to the shear capacity obtained from various models and from test results from literature. The results are used to explain the cause of failure of the integral bridge under dead load.

KEYWORDS

bridge collapse, forensic engineering, integral bridge, shear behavior, shear strength

1 | INTRODUCTION

In Wieselburg (Austria), a newly built integral concrete bridge collapsed on June 7, 2020. The bridge had not been opened to traffic yet, and fortunately, no one was injured or killed. Many factors can lead to collapse, such as forces of nature (e.g., earthquakes, floods, landslides, etc.) or human factors (e.g., design errors or construction mistakes, collisions, war and terrorism, etc.).[1] Around 12% of bridge collapses in the USA between 1989 and 2000 were due to human factors such as lack of maintenance (8.6%), construction mistakes (2.6%) or design errors (0.6%).[2] Only a few have been reported in detail, although in many cases, expert reports about collapses used for court proceedings exist. However, these documents are usually not published after court decisions. The Government of Lower Austria established an expert commission of inquiry tasked with determining the causes of the Wieselburg Bridge collapse. The second author of this paper, Johann Kollegger, lent his expertise to the commission that filed its final report in October 2020.[3] The report concluded that the collapse can be traced back to error in the design of the shear reinforcement. In order to avoid bridge collapses due to human error in future projects, it is essential to provide engineers and scientists with open access to well-documented data of bridge failures. In this paper, the authors aim to give insights into the cause of the Wieselburg Bridge collapse based on forensics and in-depth static analyses.

2 | THE WIESELBURG BRIDGE

2.1 | Description of the structure

The Wieselburg Bridge was an integral concrete bridge with a clear span of 25 m. The bridge was one of 17 bridges on the 8.4 km Wieselburg bypass in Austria. The bridge was built between September 2018 and May 2020. Figure 1 shows a longitudinal and a transverse section of the bridge. The deck slab was 23.5 m wide and 1.5 and 1.0 m high at the abutments and the center of the span,

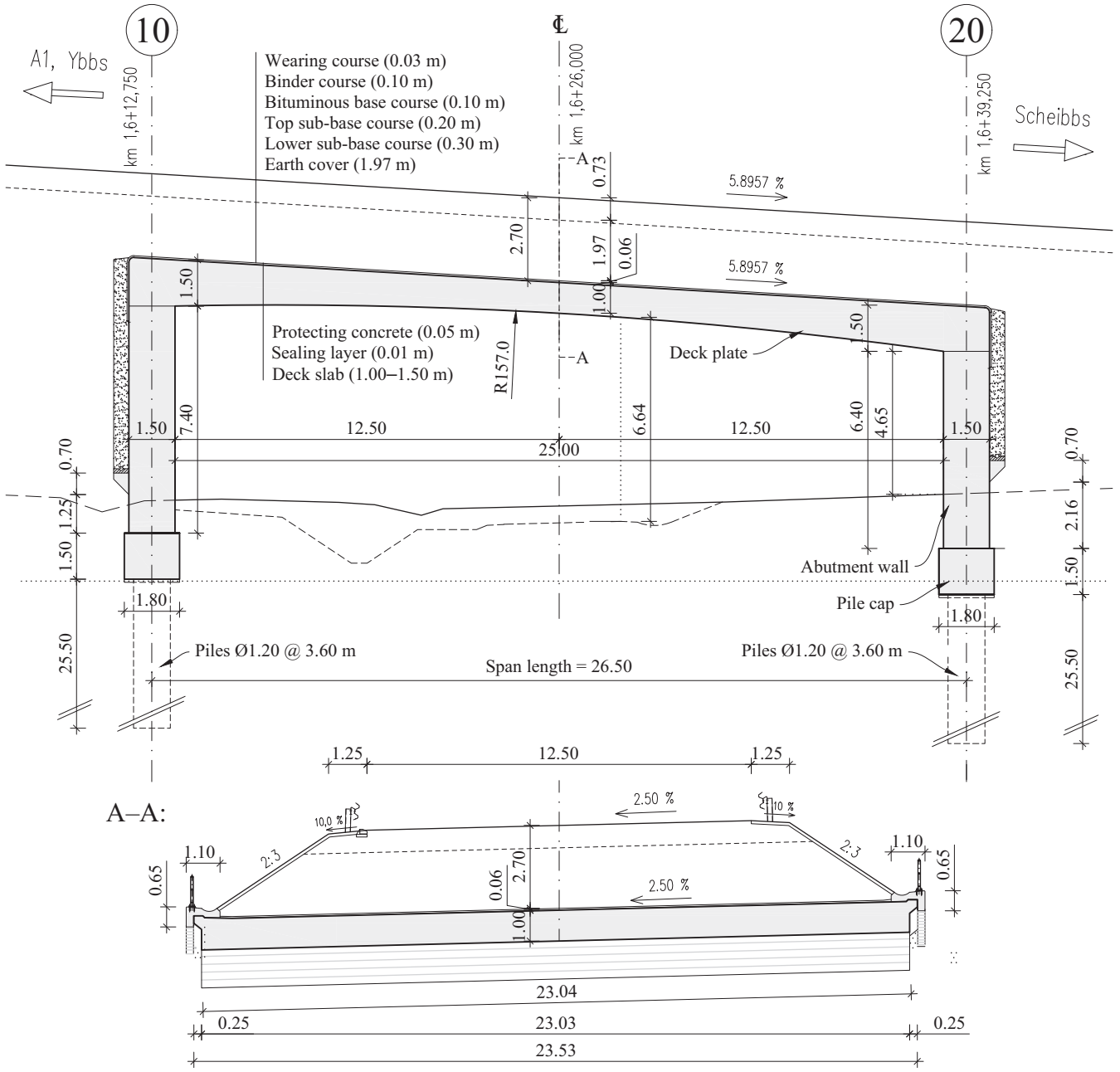

FIGURE 1 Longitudinal and transverse sections of the Wieselburg Bridge deck slab.

respectively. The bottom of the bridge deck between the abutments is curved with a radius of 157 m. The longitudinal inclination at deck level was designed to be 5.9%. The thickness of the abutment walls was 1.5 m, resulting in a total span of 26.5 m. The height of the abutment walls was 7.4 m at axis 10 and 6.4 m at axis 20 (Figure 1). Pile caps, 1.5 m high and 1.8 m wide, were located underneath the abutment walls. Seven piles with a diameter of 1.2 m, a length of 25.5 m and a center-to-center distance of 3.6 m were located at each abutment. The characteristic concrete strengths f_{ck} assumed in the design are listed in Table 1. The nominal characteristic yield strength of the reinforcement B550B was 550 N/mm^2.

As can be seen in Figure 1, the bridge was carrying a 1.97 m earth cover and a 0.73 m pavement structure. The layout of the top longitudinal reinforcement of the deck slab at abutments 10 and 20 is shown in Figure 2. The 30 mm bars spaced at 150 mm (shown in green in Figure 2) ended at distances of 3.10 and 3.65 m from axes 10 and 20, respectively. Beyond this point, only the reinforcing bars Ø26/150 mm were available to carry the tensile forces resulting from the negative moments. The

Part	Concrete class	D_{max} (mm)	c_{nom}	f_{ck} (N/mm²)
Deck slab	C25/30; XF2	—	40	25
Abutment walls	C25/30; XF2	—	40	
Pile caps	C25/30; XF3	32	40	
Piles	C25/30; XF1/XA1L/UB2	32	100	

TABLE 1 Concrete classes and characteristic compressive strengths of relevant parts of the Wieselburg Bridge.

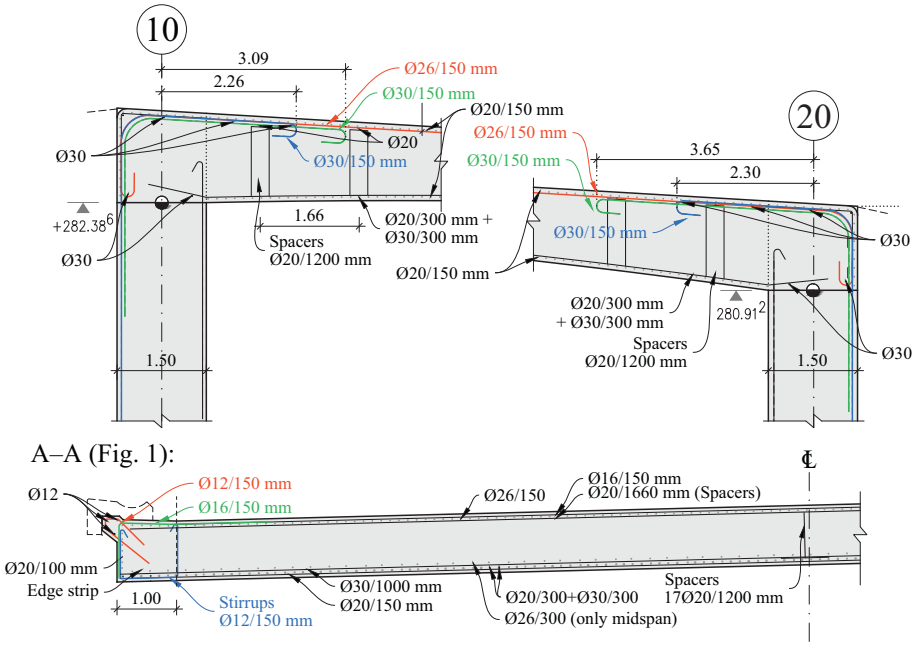

FIGURE 2 Layout of deck slab reinforcement at the abutments and in cross section at midspan.

edge strips of the slab (approximately 1 m wide) contained two-legged stirrups Ø12/150 mm. Due to a design error, no further shear reinforcement was included in the deck slab (see Figure 2). As can be seen in Figure 2, two-legged spacers Ø20/1200 mm were the only transverse reinforcement in the inner region of the deck slab. Since the spacers did not enclose the longitudinal reinforcement, they could not be considered to act as shear reinforcement. This means that the inner region of the deck slab was devoid of any shear reinforcement.

2.2 | Material properties determined after failure

After the collapse of the bridge, the strength properties of the concrete and the reinforcement, as well the weight of the earth cover, were determined.[4] Pieces of concrete from the south-west side of the collapsed bridge were collected and transported to the laboratory. In the laboratory, concrete cores with a diameter of 80 mm were extracted from the concrete pieces. The concrete cores were sawn into 80 mm long specimens. The compressive strength of the cylindrical specimens was determined according to ONR 23303.[5] A total of 22 specimens from eight concrete cores were tested. The data and results of the tests are shown in Table 2. ÖNORM EN 13791[6] stipulates that the compressive strength of concrete f_{cm} can be derived from compression test results of cylindrical specimens with a height-to-diameter ratio of 1:1 by multiplying the test results by a factor of 0.82. A mean compressive strength f_{cm} of 47.7 N/mm² with a coefficient of variation of 0.099 was obtained. The characteristic compressive strength of the concrete used in the bridge was thus determined to be 38.0 N/mm², which is greater than that of the used concrete class (see Table 1). The mean density of the concrete was 2369 kg/m³.

A total of 14 reinforcement specimens with different diameters were tested. The specimens were collected at locations where the reinforcement was exposed after the collapse of the bridge. This means that some of the specimens were subjected to large tensile forces during the collapse. The yield strength $f_{sy,0.2\%}$, defined as the offset yield point at 0.2% strain, and the ultimate strength f_{su} are listed in Table 3.

The density of the earth cover was determined at six locations behind abutment 10, from samples taken at a

TABLE 2 Concrete properties determined from fragments of the collapsed bridge.

Core	Abutment	Specimen	Density (kg/m^3)	$f_{c,1:1}$ (N/mm^2)	$f_{c,2:1}$[a] (N/mm^2)
1	10	1/1	2350	63.2	51.8
		1/2	2380	61.7	50.6
		1/3	2370	58.1	47.6
2	10	2/1	2400	65.4	53.6
		2/2	2420	65.2	53.5
		2/3	2400	60.8	49.9
3	10	3/1	2370	52.7	43.2
		3/2	2290	41.5	34.0
		3/3	2390	58.5	48.0
4	10	4/1	2360	60.9	49.9
		4/2	2380	65.1	53.4
		4/3	2350	56.1	46.0
5	10	5/1	2190	58.5	48.0
		5/2	2400	60.6	49.7
		5/3	2360	60.9	49.9
6	10	6/1	2410	65.1	53.4
		6/2	2380	48.1	39.4
		6/3	2390	53.5	43.9
7	20	7/1	2390	55.7	45.7
		7/2	2310	54.3	44.5
8	20	8/1	2400	57.7	47.3
		8/2	2420	56.1	46.0

[a] $f_{c,2:1} = 0.82 \cdot f_{c,1:1}$ according to EN 13791.[6]

TABLE 3 Strength properties of reinforcement specimens collected from the collapsed bridge.

Specimen	Type of reinforcement	Diameter (mm)	$f_{sy,0.2}$ (N/mm^2)	f_{su} (N/mm^2)	$f_{su}/f_{sy,0.2}$
1	Longitudinal bar	26	674	703	1.04
2	Stirrup	12	553	687	1.04
3	Stirrup	12	517	691	1.34
4	Stirrup	12	559	671	1.20
5	Transverse bar	16	547	648	1.18
6	Longitudinal bar	26	491	653	1.33
7	Longitudinal bar	20	576	680	1.18
8	Longitudinal bar	26	463	649	1.40
9	Longitudinal bar	20	567	674	1.19
10	Transverse bar	16	538	676	1.26
11	Transverse bar	20	567	664	1.17
12	Transverse bar	20	564	664	1.18
13	Transverse bar	20	564	668	1.18

depth of 0.15 m below the pavement structure. The soil density and the water content were measured by a Troxler nuclear moisture density gauge. The results of the measurements are contained in Table 4. The mean density of the earth cover, as determined on June 17, 2020, was 2307 kg/m^3.

TABLE 4 Density measurements of earth cover.

Specimen	Distance from the noise barrier (m)	Water content (% of mass)	Density (kg/m^3)
1	14.2	6.5	2363
2	12.2	5.9	2220
3	5.9	7.3	2322
4	4.1	4.4	2353
5	2.0	5.8	2262
6	7.6	4.5	2324

(a) (b)

FIGURE 3 Collapsed Wieselburg Bridge: (a) from the south-west; (b) from the north-east.

(a) (b)

FIGURE 4 Detailed view of the failure plane close to abutment 10: (a) end hooks of reinforcing bars; (b) flexural shear crack.

3 | THE WIESELBURG BRIDGE COLLAPSE

The Wieselburg Bridge collapsed on June 7, 2020, around 4 p.m.[3] Due to the amount of dust generated by the collapse, the failure was immediately noticed by police officers who happened to be close to the bridge. The collapse occurred under dead load only, since the bridge had not yet been opened to traffic. Fortunately, the collapse occurred on a Sunday, meaning that there were also no construction vehicles on the bridge. No one was killed nor injured.

The deck slab had been cast on August 1, 2019. At the time of the collapse, the concrete was, therefore, around 10 months old. Figure 3 shows the collapsed bridge from the south-west and the north-east sides.

A detailed view of the crack plane (abutment axis 10) where shear failure of the bridge initiated is shown in Figure 4. The end hooks of the 30 mm reinforcement bars (shown in green in Figure 2) can clearly be seen in the

(a) (b)

FIGURE 5 Tilted abutment 20 with shear crack: (a) from the south-west; (b) from the north-east.

top part of the failure plane. An analysis of the shear capacity of the deck slab at this location is presented in Section 4 of this paper. Figure 5 shows the tilted abutment at axis 20, with shear failure in the deck slab.

The failure sequence of the bridge was re-constructed based on the location and the measured lengths of the individual deck slab fragments (Figure 3) and is shown in Figure 6. Figure 6a illustrates the situation before the collapse of the bridge. It is assumed that flexural cracks close to the abutments and in the center region of the span must have formed because the calculated longitudinal stresses in the concrete at these locations were higher than the concrete's tensile strength, which was calculated as $f_{ctm} = 0.3 \cdot (f_{cm})^{2/3}$ as stipulated in Eurocode 2 (EC 2),[7] yielding $f_{ctm} = 3.97$ N/mm^2. Flexural cracks are shown qualitatively in regions where a tensile stress exceeding f_{ctm} was calculated from the results of the static analysis presented in Section 4.1 of this paper. A wide crack is shown in Figure 6a at a distance of 3.10 m from axis 10. At this location, the area of the top longitudinal reinforcement dropped from 8252 to 3540 mm^2/m (see Figure 2). It is important to note, that the same decrease in longitudinal reinforcement occurs at a distance of 3.65 m from axis 20; however, this location is located in the uncracked region at the beginning of the failure sequence.

The flexural shear crack that developed from the flexural crack at a distance of 3.10 m from axis 10 triggered the collapse of the bridge (Figure 6b). With the development of the flexural shear crack, the bridge was separated into two parts which were connected only by the top longitudinal reinforcement (26 mm bars spaced at 150 mm, shown in red in Figure 2) and the bottom longitudinal reinforcement (20 mm bars spaced at 300 mm, shown in black in Figure 2). The left part of the new structural system consisted of the abutment wall at axis 10 and a short cantilevering part of the deck slab. The right part comprised the abutment wall at axis 20, which was supported by seven piles, and a long (almost 24 m) cantilevering part of the deck slab. The long cantilever of the right part caused a significant increase in bending moment in the frame corner and the abutment wall at axis 20, notably increasing shear in the deck slab. The large bending moment exceeded the load-carrying capacity of the seven piles at axis 20 and caused bending failure of the piles beneath the pile cap. As a consequence of the high shear in the deck slab, a flexural shear crack formed at a distance of 3.65 m from axis 20, as can be seen in Figure 6c. After plastic hinges formed at the top of the piles at axis 20, the right part of the bridge was no longer stable and started moving to the left toward axis 10. During this movement, the tip of the cantilever was still supported by the top and bottom longitudinal reinforcement, which was anchored in the left part of the bridge. The tensile forces in the top longitudinal reinforcement caused spalling of the concrete cover and facilitated the movement of the right part toward axis 10. The bottom longitudinal reinforcement was strongly anchored in both parts of the structure: in the frame corner of the left part of the bridge at axis 10 and in the concrete of the tip of the cantilever in the right part of the bridge, where the tensile forces of the reinforcement caused upward-acting compressive stresses in the concrete. Eventually, the tip of the cantilever of the right part of the bridge touched the abutment wall at axis 10. In the following step of the collapse mechanism, shown in Figure 6d, the tensile force in the top longitudinal reinforcement caused further spalling of the concrete and a separation of the top reinforcement from the deck slab. The tip of the cantilever of the right bridge part stayed in contact with the abutment wall in axis 10 because the bottom longitudinal reinforcement was still able to sustain the axial forces acting at the tip of the cantilever. Further bending cracks developed close to the top of the cantilever due to the

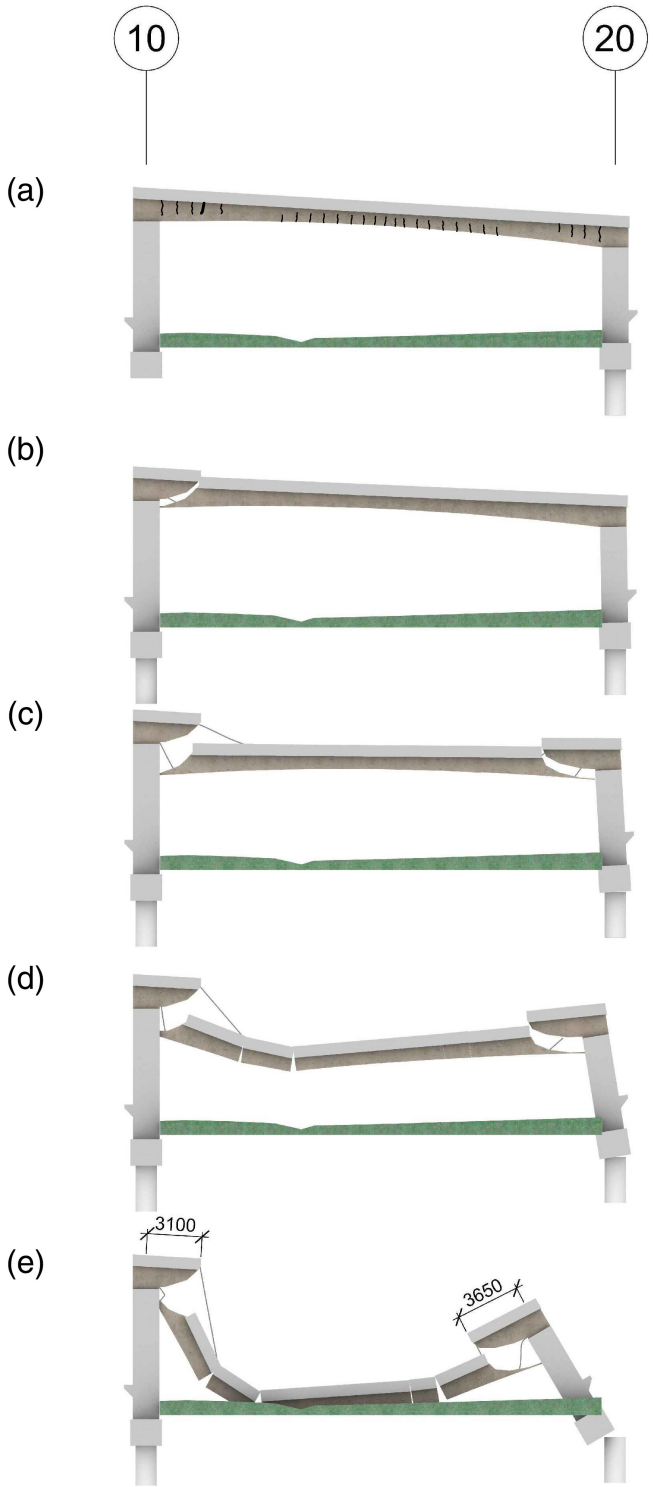

FIGURE 6 Re-construction of the collapse sequence triggered by flexural shear failure close to axis 10.

high dead load and the changed structural system. The tensile forces in the bottom longitudinal reinforcement caused further tilting of the abutment at axis 20. The tilting of the abutment at axis 20 kept increasing until the deck slab touched the ground, as shown in Figure 6e. As a consequence of the leftward movement of the right part of the bridge and the contact of the tip of the cantilever with the abutment wall in axis 10, an upward movement of the tip occurred. This movement led to the buckling of the bottom longitudinal reinforcement, as can be seen in Figure 4. In both the right and left parts of the bridge, the top and bottom longitudinal reinforcement crossing the flexural shear crack close to axis 20 were still connecting the individual pieces of the collapsed bridge (see also Figure 5).

4 | STRUCTURAL ANALYSIS OF THE COLLAPSING BRIDGE

4.1 | Static analysis of the bridge structure

In planar members, such as solid slabs, the shear forces are generally not constant over their width, with the peak values occurring at the edges or around concentrated loads. Thus, shear design is usually performed separately for an inner and an outer slab strip, using averaged shear force values. For the Wieselburg Bridge, the edge strips were designed with a small amount of shear reinforcement (stirrups Ø12/150 mm, see Figure 2), and the dead load was equally distributed over the inner region of the slab (Figure 1). Therefore, a simple two-dimensional static analysis was carried out to determine the representative internal forces for the inner slab strip. The analyzed section of the bridge has a width of 3.6 m, corresponding to the center-to-center spacing of the piles. The dead load acting on the deck slab of the bridge was determined from the measurements presented in Section 3 or from the nominal weights of the materials. The loads are summarized in Table 5 for a 1.0 m high section at midspan.

The loads applied in the numerical model of the bridge are illustrated in Figure 7. The horizontal earth pressure was determined by assuming a soil density of 2307 kg/m^3, corresponding to the density of the earth cover, and considering an earth pressure at rest with a factor of $K_0 = 0.5$. The horizontal stiffness C_x of the soil for the support of the piles was set to 40 MN/m^3 according to the information in the geotechnical report. This value was multiplied by the diameter of the pile (1.2 m) in order to model the pile as a member with elastic support. The stiffness was assumed to increase parabolically, starting at 1 m depth below the pile head and reaching 100% at 5 m. In a study where $C_x = 20$ MN/m^3 and $C_x = 80$ MN/m^3 were assumed, it was found that the assumed value of C_x had a very small influence on the member forces in the deck slab of the bridge.

TABLE 5 Loads acting on a 1.0 m wide strip of the bridge deck slab.

Material	Thickness (m)	Weight (kN/m^3)	Load (kN/m^2)	Line load (kN/m)
Wearing course	0.03	24	0.72	0.72
Binder course	0.1	24	2.4	2.4
Bituminous base course	0.1	24	2.4	2.4
Top subbase course	0.2	23	4.6	4.6
Lower sub-base course	0.3	23	6.9	6.9
Earth cover	1.97	22.6	44.6	44.6
Protecting concrete	0.05	22	1.1	1.1
Sealing layer	0.01	10	0.1	0.1
Concrete	1.0–1.5	23.2	23.2	23.2–34.8
Reinforcement	—	77.1	0.94	0.94–1.41
Sum	3.76–4.26	—	—	86.96–99.03

The calculated bending moments, shear forces, and axial forces due to the loads shown in Figure 7 are displayed in Figure 8 for a 1 m wide section of the deck slab. The maximum values of the internal forces are shown, as well as the internal forces at the two critical locations where the top longitudinal Ø30 mm reinforcing bars ended (see Figure 2).

4.2 | Shear capacity of the deck slab according to Eurocode 2

The shear capacity $V_{Rm,c}$ of the deck slab with a width b_w equal to 1.0 m was calculated according to EC 2[7] using mean material properties and the unfactored axial forces:

$$V_{Rm,c} = \left[\frac{C_{R,c}}{\gamma_c} \cdot k \cdot (100 \cdot \rho \cdot f_{cm})^{\frac{1}{3}} + k_1 \cdot \sigma_{cp}\right] b_w \cdot d \quad (1)$$

The empirical factor $C_{R,c}$ was set to 0.15 according to the recommendations by König[8] for posttest analysis. The partial safety factor γ in Equation (1) was taken as 1.0. The factor for size effect k was determined with

$$k = 1 + \left(\frac{200}{d\,[\text{mm}]}\right)^{\frac{1}{2}}. \quad (2)$$

The effective height d varied over the length of the bridge and was calculated using the dimensions in the structural drawings (Figures 1 and 2).

The reinforcement ratio

$$\rho = \frac{A_{sl}}{b_w \cdot d} = \frac{\sum A_{s,eff}}{b_w \cdot d} \quad (3)$$

was calculated using the effective area of the tensile reinforcement A_{sl} determined at the distance d from the control section (CS) considered (see continuous lines in Figure 9).

Note that the anchorage conditions of the reinforcing bars acting in the considered cross-section are used in the determination of A_{sl} by using

$$A_{s,eff} = A_s \frac{l_{b,eff}}{l_{bm}} \leq A_s, \quad (4)$$

where $l_{b,eff}$ is the effective anchorage length of a reinforcing bar available beyond the distance d from the considered section (see Figure 9), and l_{bm} is the mean value of the required anchorage length determined with the formulas given in EC 2[7]:

$$l_{bm} = \frac{Ø}{4} \cdot \frac{f_y}{f_{bm}} \cdot \alpha_i \text{ and } f_{bm} = 2.25 \cdot \eta_1 \cdot \eta_2 \cdot f_{ctm}, \quad (5)$$

where f_y is the mean value of the yield strength of the reinforcing bar, α_i are coefficients to account for improved anchorage conditions (e.g., type of anchorage, concrete cover, transverse reinforcement), f_{bm} is the mean bond strength, η_1 is a coefficient considering the quality of the bond condition and the position of the bar during concreting and η_2 accounts for the bar diameter.

For the longitudinal reinforcement (Ø26 and Ø30 mm) at the top of the slab, $\eta_1 = 0.7$ due to the poor bond conditions in the top 300 mm of concrete and $\eta_2 = 1.0$ for bars with a diameter below 32 mm. The yield strength was set to the nominal value of 550 N/mm^2. For the hooks at the ends of the reinforcing bars cantilevering from the abutment, a coefficient $\alpha_1 = 0.7$ was assumed

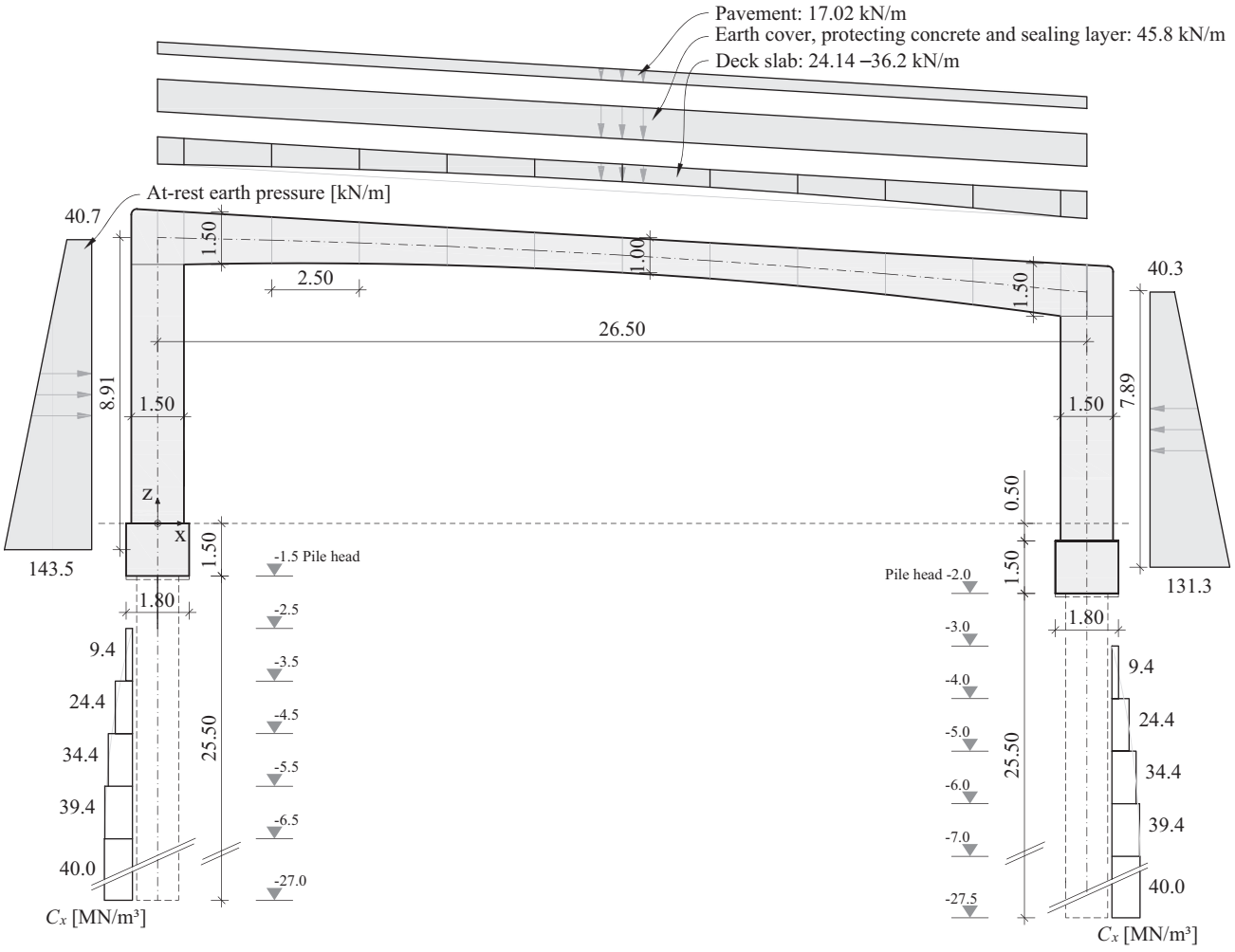

FIGURE 7 Loads on the numerical model of the bridge, shown for a 1.0 m wide section.

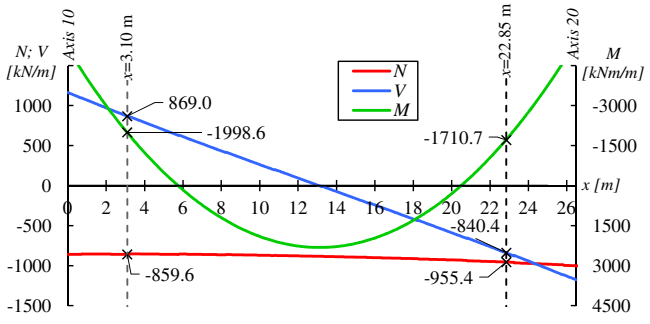

FIGURE 8 Bending moments (green), shear forces (blue) and axial forces (red) due to dead load for a 1 m wide section of the deck slab.

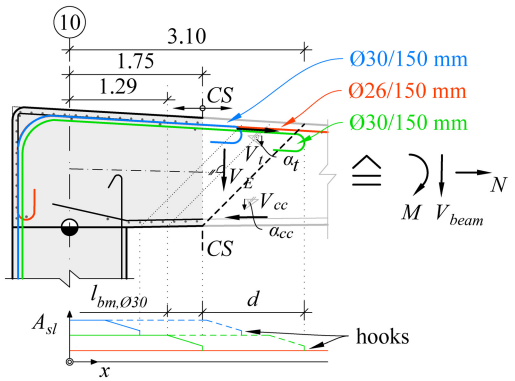

FIGURE 9 Considerations for shear capacity determination in a control section (CS) according to EC 1992-1-1[7]: effective area of tensile reinforcement A_{sl} and share of the shear force carried by the compression chord (V_{cc}) and the tension chord (V_t).

since the distances between the hooks meet the requirements according to EC 2. A mean concrete compressive strength of 47.7 N/mm^2 as described in Section 2.2 of this paper was used in Equation (1). The mean tensile strength was calculated as $f_{ctm} = 0.3 \cdot (f_{cm})^{2/3}$ according to EC 2,[7] yielding $f_{ctm} = 3.97$ N/mm^2. Applying the parameters described above in Equations (4) and (5), the mean values of the required anchorage length l_{bm} are 402 and 464 mm for 26 and 30 mm bars, respectively.

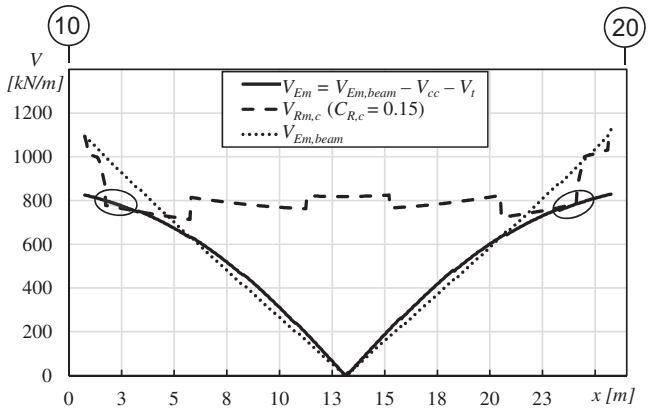

FIGURE 10 Shear capacity $V_{Rm,c}$ and shear forces $V_{Em,beam}$ calculated according to beam theory and actual shear forces V_{Em} for a 1.0 m wide section of the Wieselburg Bridge deck slab.

The axial stress

$$\sigma_{cp} = \frac{N}{b_w \cdot h} \tag{6}$$

was calculated with the axial forces shown in Figure 8 for width $b_w = 1.0$ m and the height of each section. The factor k_1 was set to 0.15 according to EC 2.[7] Due to the normal force ranging between −854.7 and −988.4 kN along the inclined axis, σ_{cp} varies from −0.60 N/mm^2 (abutment 10) to −0.97 N/mm^2 (midspan).

Figure 10 shows a comparison of the shear capacity $V_{Rm,c}$ and the shear forces for a 1 m wide deck slab section of the Wieselburg Bridge. The dashed line in Figure 10 represents the shear capacity $V_{Rm,c}$ calculated as explained above. The dotted line in Figure 10 corresponds to the shear force $V_{Em,beam}$ shown in Figure 8. This shear force has to be adjusted according to the stipulations given in, EC2[7] and Zilch et al.[9] as the tension and compression chords were not parallel to the axis of the deck slab (see Figure 9). Thus, the shear force V_{Em}, which had to be carried by the web of the deck slab, is calculated as

$$V_{Em} = V_{Em,beam} - V_{cc} - V_t, \tag{7}$$

where $V_{Em,beam}$ is the total shear force calculated in the beam model, V_{cc} is the share of the shear force carried by the compression chord and V_t is the share carried by the tension chord. The individual components were calculated as $V_{cc} = M/z \cdot \tan \alpha_{cc}$ and $V_t = M/z \cdot \tan \alpha_t$. Note that the normal force N is already considered in Equation (1). As can be seen in Figure 10, the actual shear force V_{Em} is smaller than the shear force $V_{Em,beam}$, which was calculated with a finite element program using beam elements in the regions next to the abutment sustaining negative bending moments. In the middle part of the slab where positive bending moments occur (see Figure 8), the actual shear force V_{Em} is larger than the shear force $V_{Em,beam}$ calculated according to beam theory.

From the results presented in Figure 10, it can be seen that the shear capacity $V_{Rm,c}$ calculated with Equation (1) according to EC 2[7] is only slightly larger than the actual shear force V_{Em} occurring at the sections at distances of 1.75 and 2.40 m from the axis of abutments 10 and 20, respectively. These sections correspond to the exact locations at which the bars protruding from the abutment could no longer be considered in Equation (3) (see Figure 9). The ratios $V_{Em}/V_{Rm,c}$ are 1.03 and 1.00 for the critical failure planes next to abutments 10 and 20, respectively. As has been explained in Section 2, the failure occurred in the critical failure plane next to abutment 10.

4.3 | Analysis of the flexural capacity

Nonlinear cross-section analysis was performed using the INCA2 software,[10] assuming a bilinear stress–strain relationship for the reinforcement and a parabolic relationship for concrete under compression as specified in EC 2.[7] The material properties listed in Tables 2 and 3 were used and the Young's modulus of steel was set to $E = 200{,}000$ N/mm^2. The analysis was performed on several relevant sections in the vicinity of the failure plane near abutment 10. The effective tensile reinforcement in the analyzed cross section was calculated considering the anchorage conditions described in Section 4.2., but without accounting for the distance d for an inclined flexural shear crack (dashed lines in Figure 9). The calculated stresses in the concrete and the reinforcement due to the internal forces (N and M from Figure 8) are summarized in Table 6.

The results show that the bridge deck had sufficient flexural strength to sustain the dead load (Table 5), as the calculated stresses are generally below the material strengths obtained from tests (Tables 2 and 3). Nevertheless, very high tensile stresses (362.4 N/mm^2) occurred, due to the bending moment ($M = -1998.6$ kN/m) and the axial force ($N = -859.6$ kN/m) acting at the section where the reinforcement ended ($x = 3.10$ m). The results indicate that the reinforcement layout (see Figure 2) was not designed correctly, as these high stresses would lead to large crack widths even in the serviceability limit state (see Section 4.4). It is important to note that even if no axial force were to act within this section, the flexural capacity would not be reached (Table 6).

TABLE 6 Stress state in several cross sections at abutment 10 calculated for a width of 1.0 m.

x (m)	M (kNm)	N (kN)	d (m)	A_{sl} (mm²)	σ_c (N/mm²)	σ_s (N/mm²)	c (mm)
0.75	−4287.7	−854.7	1.42	12,964	−16.7	226.4	417
1.75	−3242.3	−856.7	1.34	12,964	−14.1	176.2	412
2.35	−2677.2	−857.9	1.30	8252	−14.4	222.1	343
3.09	−1998.6	−859.6	1.25	4953	−13.9	263.6	283
3.10	−1998.6	−859.6	1.25	3540	−15.7	362.4	240
3.10	−1998.6	0[a]	1.25	3540	−15.6	477.1	193

[a]Hypothetical case.

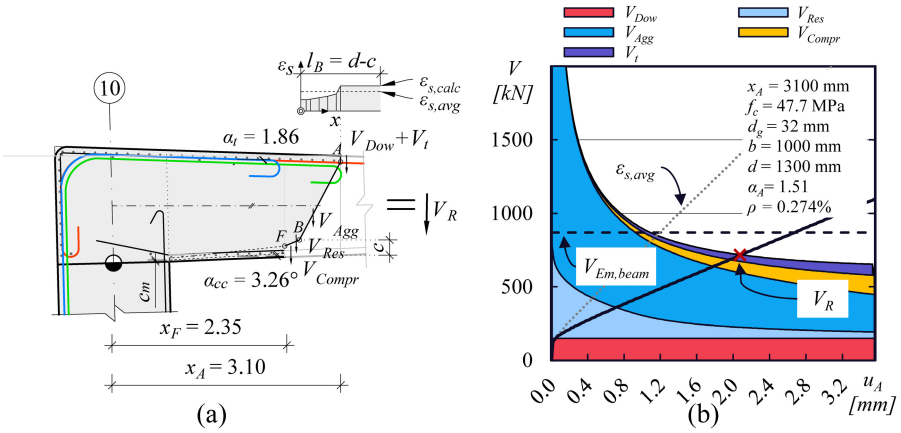

FIGURE 11 Shear capacity determined with the shear model proposed in Cavagnis et al.[12]

4.4 | Modeling based on shear transfer actions

The shear capacity of slender members without shear reinforcement is due to several shear transfer actions, which can be described by crack kinematics of a rotating flexural shear crack.[11] At lower loads, flexural cracks develop almost vertically with their inclination influenced by the acting moment-to-shear ratio. When the flexural crack reaches the concrete compression zone, the inclination of the crack changes due to the stress state and the crack propagates almost horizontally until the shear capacity is reached.

Considering the observed shape of the failure plane (Figure 4), it seems appropriate to use a bilinear curve to represent the shear crack. The empirically derived bilinear idealization proposed by Cavagnis et al.[12] was used to analyze shear transfer actions. The inclination of the quasi-vertical part (A and B in Figure 11) is dependent on the moment-to-shear ratio (M/V) and the axial forces (N), and is calculated with

$$\beta_{AB} = \frac{\pi}{4} \cdot \left(1 + \frac{\alpha_A^{1/3}}{3}\right), \tag{8}$$

where $\alpha_A = (M_A/V_A + N/V \cdot d/3)/d$ is the shear slenderness ratio for beams subjected to axial forces.

The internal forces at $x_A = 3.10$ m ($N = -859.6$ kN; $M = -1998.6$ kNm; $V = 869.0$ kN) correspond to a shear slenderness ratio $\alpha_A = 1.51$ and an angle $\beta_{AB} = 62.2°$. The end point B of the quasi-vertical crack part is defined as the location where the compression zone height is reached ($c = 240$ mm; see Table 6). The quasi-horizontal part starts at point B, has a fixed length $l_F = d/6$, and is inclined by $\beta_{BF} = \pi/8$. The second part of the curve (B–F in Figure 11) defines the crack tip F at a distance of $x_F = 2.35$ m. The shear crack, as well as the relevant angles of the compression and tension chords, are shown in Figure 11.

The shear crack kinematics (w, s) at each point along this crack (A–B–F) can be defined by the rotation ψ of this crack around a center of rotation, which is defined as crack tip F. By imposing a certain horizontal crack opening $u_A = \psi \cdot d_F$ at the location of the longitudinal reinforcement, various constitutive models for shear transfer mechanisms which consider crack kinematics as input parameters can be evaluated (V_{Agg}, V_{Dow}, and V_{Res}). The contribution of the chords to the shear strength can be estimated by an empirically derived formula for

TABLE 7 Calculated contributions of shear transfer actions according to the proposed modeling approach (based on the study by Cavagnis et al.[12]).

V_t (kN)	V_{Agg} (kN)	V_{Res} (kN)	V_{Compr} (kN)	V_{Dow} (kN)	ΣV_i (kN)
44.8 (6%)	370.0 (52%)	74.0 (10%)	78.5 (11%)	150.1 (21%)	717.4 (100%)

compression (V_{Compr}),[12] and by taking into account the inclination of the tensile reinforcement (V_t). The sum of these individual contributions (V_i) yields the shear resistance for a certain crack width, from which a shear resistance function $V_R = \Sigma V_i(u_A)$ can be derived. It should be noted that the proposed approach is valid only for regions where no direct struts (e.g., in the region near supports or point loads) are acting within the web. For the evaluation conducted in this study, the same constitutive laws[12–16] as those proposed in Cavagnis et al.[12] were used to evaluate the shear transfer actions attributed to the concrete. The equations are given in Appendix Table A1.

Finally, the shear resistance of the considered section can be determined with a load–critical shear crack relationship as proposed in Cavagnis et al.[12]:

$$u_A = \varepsilon_s \cdot l_B = \varepsilon_s \cdot (d - c) \text{ where } \varepsilon_s = f(M_F) \text{ and } c = f(M_F) \quad (9)$$

The strains ε_s in the reinforcing bars, as well as the compression zone height c under a given bending moment M_F, were calculated numerically with INCA2[10] using the material models introduced in Section 4.3. Inserting the obtained values (ε_s, c) into Equation (9) yields the horizontal opening u_A corresponding to M_F. The related shear force is then calculated using the relationship $V_A = M_F/3.081$ determined in the static analysis presented in Section 4.1. The relationship also allows the contributions of the chords (V_{cc} and V_t) for a given horizontal opening u_A to be determined.

As can be seen in Figure 11, some contributions (namely those due to aggregate interlock and fracture process zone) decrease when the horizontal opening u_A increases, while others (due to chord actions) increase. Aggregate interlock (shown in blue in Figure 11) is the most relevant mechanism for the proposed crack geometry. The influence of the fracture process zone (shown in light blue in Figure 11) decreases significantly with increasing values of u_A, whereas the contribution of the compression zone increases with increasing values of u_A, but is also relatively small since the distance to the abutment wall is rather large (marked in yellow in Figure 11). The contribution of dowel action of the longitudinal reinforcement (shown in red in Figure 11), on the other hand, is quite significant due to the continuous load acting at the tension side of the member ($k_b = 1.0$; see Appendix Table A1).

The model yielded a shear resistance $V_R = 717.4$ kN for $u_A = 2.04$ mm (Figure 11). The corresponding contributions of the various shear transfer actions are given in Table 7.

While the shear force at $x_A = 3.10$ m was calculated to be $V_{Em,beam} = 869.0$ kN, the modeling approach slightly underestimates this value ($V_{Em,beam}/V_R = 1.21$). It is important to note that the reinforcement ratio $\rho_l = 0.27\%$ (Ø26/150 mm) was used to compute the strains ε_s. However, the tributary length l_B in Equation (9) was calibrated on beams with continuous reinforcement. Due to the location of the reinforcement cutoff point, the input parameters (ε_s, c) for Equation (9) vary in this region. Other test series on beams with curtailed reinforcement also showed the development of critical cracks at the vicinity of the reinforcement cutoff point.[17,18] If the strains are calculated based on the varying amounts of longitudinal reinforcement A_{sl} as shown in Figure 9 and then averaged over the tributary length l_B, the modeling approach yields a more accurate result (shown as a dotted gray line in Figure 11b).

4.5 | Comparison of the shear capacity of the Wieselburg Bridge with other test results

The failure of the Wieselburg Bridge can be regarded as a large and expensive shear test with the shear failure of a thick deck slab under uniform load. In recent years, the structural assessment of existing structures has become highly relevant and structural assessment analyses frequently show bridges to have insufficient shear capacity[19] due to reasons such as today's higher traffic loads, more conservative shear models, or insufficient detailing. However, in the book on failed bridges by Scheer,[20] not a single bridge collapse due to shear failure has been reported. Mitchell et al.[21] describe the failure of the Concorde overpass in Laval, Canada, and discuss its structural aspects, which were also discussed by Golden et al.[22] In this overpass, shear failure occurred in a 1.156 m thick cantilevering slab. The 4 m cantilever was built without any shear reinforcement and was loaded at the cantilever tip where the central part of the bridge was supported by elastomeric bearings. The failure occurred under dead load and very moderate live load, 36 years after the bridge had been built. Numerous test results of beams and uniaxially loaded slab strips without shear reinforcement are also

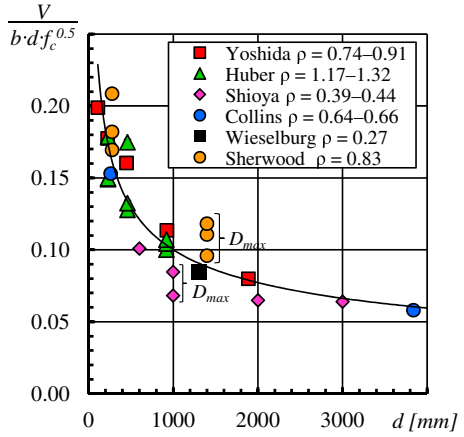

FIGURE 12 Normalized shear capacity of the critical section of the Wieselburg Bridge deck slab as a function of effective height and shear test results from literature.[23–27]

available in the literature. The results of several tests[23–27] in which the depth of the specimens was varied are displayed in Figure 12.

As can be seen from the results shown in Figure 12, the shear capacity obtained from static analysis (Section 4.1) shows good agreement with those of the other test series. Furthermore, it can be seen that the deck slab of the Wieselburg Bridge had a low flexural reinforcement ratio (as discussed in Section 4.3) compared to the other tests, and only a few tests had a static depth larger than the critical section of the Wieselburg Bridge ($d = 1300$ mm according to the crack geometry proposed in Section 4.4). It is important to note that the displayed results from other literature contain only tests on specimens with single point loads and constant cross-section depth in which no axial forces were present. However, the normal stress at the critical cross section of the Wieselburg Bridge was only 0.66 N/mm^2 according to Section 4.1.

5 | SUMMARY AND CONCLUSIONS

This paper deals with the collapse of the Wieselburg Bridge, with a focus on the shear capacity at collapse load. Based on the findings of this analysis, the following conclusions are drawn:

- Shear failure at the taller abutment triggered a second shear failure with a simultaneous flexural failure of the piles at the other abutment. The collapse sequence was re-constructed based on (a) photographs from the collapsed bridge, (b) on-site geometry measurements, and (c) static analysis using (d) material properties determined from tests of material samples from the collapsed bridge.
- Shear failure as the primary cause of failure was confirmed by comparing the analytical shear strength calculated according to Eurocode 2 to the internal forces determined for the inner slab strip. The results of the analysis were confirmed by assessing various shear transfer mechanisms of a proposed shear crack geometry and by comparing the calculated shear strength with other tests from literature.
- A modeling approach based on the work of Cavangis et al.[12] for the assessment of the relevance of various shear transfer mechanisms shows good agreement between the assumed crack geometry and the failure plane observed in the collapsed bridge. However, the calculated mean value to the shear resistance slightly underestimates the ultimate shear resistance calculated from the actual situation at failure. Further investigations on the effect of a reinforcement cutoff point on the load–critical shear crack relationship are necessary to further refine the model. The model shows that the main contribution to shear transfer can be attributed to aggregate interlock.
- Flexural failure of the deck slab was excluded as a failure cause based on the conducted nonlinear cross-section analysis. The analysis highlights an additional design error, apart from the missing shear reinforcement, showing that high tensile stresses under serviceability limit state occur in the reinforcement due to the location of the cutoff point of the reinforcement protruding from the abutment wall.

NOMENCLATURE

A_{sl}	effective cross-section area of the longitudinal reinforcement
$C_{R,c}$	empirical factor for shear capacity according to Eurocode 2
C_x	horizontal stiffness
D_{max}	maximum aggregate size
EC 2	Eurocode 2
N	normal force
M	bending moment
V	shear force
V_{Agg}	contribution of aggregate interlock to the shear strength
V_{Compr}	contribution of compression chord to the shear strength
V_{Dow}	contribution of dowel action of the longitudinal reinforcement to the shear strength
V_{Res}	contribution of residual tensile stresses in the fracture process zone to the shear strength

V_{cc}	shear carried by an inclined compression chord
V_t	shear carried by an inclined tensile chord
$V_{R,c}$	shear resistance of members without shear reinforcement
b_w	width
c	compression zone height
d	static depth
f_c	concrete cylinder compressive strength
f_{bm}	mean value of the bond strength
f_{ck}	characteristic value of concrete cylinder compressive strength
$f_{sy,0.2\%}$	yield strength of the reinforcing bar defined as the offset yield point at 0.2% plastic strain
f_{su}	ultimate tensile strength of the reinforcing bar
h	height
k	size factor
k_1	factor accounting for normal stresses
l_B	length contributing to shear crack opening; tributary length
l_{bm}	mean value of the required anchorage length
$l_{b,eff}$	effective anchorage length of a reinforcing bar beyond the distance d from the considered section
m	mean value
u	horizontal opening, i.e., the horizontal distance between opposite crack faces
α_i	coefficients to account for improved anchorage conditions
β	idealized crack angle
ρ	longitudinal reinforcement ratio
η_1	coefficient to account for the quality of the bond conditions
η_2	coefficient to account for the bar diameter
σ_{cp}	normal stress calculated for the cross section
σ	normal stress parallel to the beam axis
τ	shear stress

AUTHOR CONTRIBUTIONS

Conceptualisation, methodology, writing—original draft preparation: Tobias Huber and Johann Kollegger; *formal analysis and structural assessment*: Tobias Huber and Johann Kollegger; *shear capacity evaluation*: Tobias Huber and Patrick Huber; *forensics*: Dominik Suza and Johann Kollegger; *review and editing*: Tobias Huber, Dominik Suza, Patrick Huber, and Johann Kollegger; *project administration, supervision*: Johann Kollegger. All authors have read and agreed to the published version of the manuscript.

ACKNOWLEDGMENTS

The authors acknowledge TU Wien Bibliothek for financial support through its Open Access Funding Program.

CONFLICT OF INTEREST STATEMENT

The authors declare that there are no conflicts of interest.

DATA AVAILABILITY STATEMENT

The data that support the findings of this study are available from the corresponding author upon reasonable request.

ORCID

Tobias Huber https://orcid.org/0000-0001-9248-1662
Patrick Huber https://orcid.org/0000-0002-7441-0200

REFERENCES

1. Deng L, Wang W, Yu Y. State-of-the-art review on the causes and mechanisms of bridge collapse. J Perform Constr Facil. 2016;30(2):04015005.
2. Wardhana K, Hadipriono F. Analysis of recent bridge failures in the United States. J Perform Constr Facil. 2003;17(3):144–50.
3. Kollegger, J. and Schweighofer, B. Endbericht der Expertenkommission zum Einsturz der Brücke B25.14 der Umfahrung Wieselburg (Final report of the expert committee on the collapse of the bridge B25.14 of the bypass Wieselburg), German, Vienna. St.Pölten: Authorities of Lower Austria, Report ST1-SC-40/002-2020. 2020.
4. Pamminger R. Prüfbericht über die Materialprüfungen im Zuge einer Bauwerksprüfung am bestehenden Brückenobjekt B25.14. Materialprüfanstalt Hartl, Report 011445/1. 2020.
5. ONR 23303. Test methods for concrete—national application of testing standards for concrete and its source materials. Vienna: Austrian Standards; 2010.
6. ÖNORM EN 13791. Assessment of in-situ compressive strength in structures and precast concrete components; German version. Vienna: Austrian Standards; 2019.
7. EN 1992-1-1. Eurocode 2: design of concrete structures, part 1–1: general rules and rules for buildings. Brussels: European Committee of Standardization (CEN); 2004.
8. König G, Fischer J. Model uncertainties concerning design equations for the shear capacity of concrete members without shear reinforcement. CEB Bulletin. 1995;224:49–100.
9. Zilch K, Zehetmaier G. Bemessung im konstruktiven Betonbau: nach DIN 1045–1 (Fassung 2008) und EN 1992-1-1 (Eurocode 2). Berlin, Heidelberg: Springer-Verlag; 2009.
10. Pfeiffer U. Inca 2: Interactive Nonlinear Cross-Section Analysis Bilinear; v2.9.0. 2019. Accessed 24 February 2023. Available from: https://www.u-pfeiffer.de/
11. Muttoni A, Ruiz MF, Cavagnis F. Shear in members without transverse reinforcement: from detailed test observations to a mechanical model and simple expressions for codes of practice. fib Bulletin. 2018;85:7–23.
12. Cavagnis F, Ruiz MF, Muttoni A. A mechanical model for failures in shear of members without transverse reinforcement based on development of a critical shear crack. Eng Struct. 2018;157:300–15.
13. Reinhardt HW. Fracture mechanics of an elastic softening material like concrete. Heron. 1984;29(2):1–42.
14. Walraven JC. Fundamental analysis of aggregate interlock. J Struct Div. 1981;107(11):2245–70.
15. Guidotti R. Poinçonnement des planchers-dalles avec colonnes superposées fortement sollicitées. PhD thesis. Thesis no. 4812

(in French). Lausanne, Switzerland: Ecole Polytechnique Fédérale de Lausanne; 2010. p. 416.
16. Fernández Ruiz M, Mirzaei Y, Muttoni A. Post-punching behavior of flat slabs. ACI Struct J. 2013;110:801–12.
17. Baron MJ. Shear strength of reinforced concrete beams at points of bar cutoff. J Am Concr Inst. 1966;63-6:127–34.
18. Leonhardt F, Walther R. Schubversuche an einfeldrigen Stahlbetonbalken mit und ohne Schubbewehrung. Deutscher Ausschuss für Stahlbeton (in German). Volume 151. Berlin: Ernst & Sohn; 1962. p. 1–83.
19. Fischer O, Müller A, Lechner T, Wild M, Kessner K. Findings and insights concerning the results of re-analyzed concrete bridges in Germany (in German). Beton-Stahlbetonbau. 2015; 109(2):107–27.
20. Scheer J. Failed bridges: case studies, causes and consequences. Hoboken, NJ: John Wiley & Sons; 2011.
21. Mitchell D, Marchand J, Croteau P, Cook WD. Concorde overpass collapse: structural aspects. J Perform Constr Facil. 2011; 25(6):545–53.
22. Golden J, Gomes E, Roy A, Su Y. De La Concorde overpass bridge collapse: analysis of a historical failure, Technical Report ME224, University of California (Berkeley). 2018.
23. Yoshida Y. Shear reinforcement for large lightly reinforced concrete members. MASc thesis. Toronto, CA: University of Toronto; 2000.
24. Huber P, Huber T, Kollegger J. Investigation of the shear behavior of RC beams on the basis of measured crack kinematics. Eng Struct. 2016;113:41–58.
25. Shioya T, Iguro M, Nojiri Y, Akiyama H, Okada TJSP. Shear strength of large reinforced concrete beams. ACI Special Publication. 1990;118:259–80.
26. Collins MP, Bentz EC, Quach PT, Proestos GT. The challenge of predicting the shear strength of very thick slabs. Concr Int. 2015;37(11):29–37.
27. Sherwood EG, Bentz EC, Collins MP. Evaluation of shear design methods for large, lightly-reinforced concrete beams. Advances in engineering structures, mechanics & construction. The Netherlands: Springer; 2006. p. 153–64.

AUTHOR BIOGRAPHIES

Tobias Huber, Institute for Structural Engineering, Vienna University of Technology, Vienna, Austria. Email: tobias.alexander.huber@tuwien.ac.at

Johann Kollegger, Institute for Structural Engineering, Vienna University of Technology, Vienna, Austria. Email: johann.kollegger@tuwien.ac.at

Dominik Suza, Institute for Structural Engineering, Vienna University of Technology, Vienna, Austria. Email: suza@fcp.at

Patrick Huber, Institute for Structural Engineering, Vienna University of Technology, Vienna, Austria. Email: patrick.huber@tuwien.ac.at

How to cite this article: Huber T, Kollegger J, Suza D, Huber P. The Wieselburg Bridge collapse—Analysis of the shear capacity based on forensic data. Structural Concrete. 2024;25(4): 2784–99. https://doi.org/10.1002/suco.202301005

APPENDIX A: Calculation of shear transfer actions

TABLE A1 Calculation of the contributions of the different shear transfer mechanisms.

Shear transfer action	Literature	Parameters
Residual tensile strength contribution V_{Res} $V_{Res} = f_{ct} \cdot b \cdot \cos\beta_{BF} \cdot l_{F1} \cdot \left(1 - \frac{1}{1+c_1} \cdot \left(\frac{u_A \cdot l_{F1}}{d_F \cdot w_c}\right)^{c_1}\right)$ where $w_c = G_F / f_{ct} \cdot (1+c_1)/c_1$ and $G_F = 0.073 \cdot f_c^{0.18}$	Tensile softening behavior[13]	c_1: constant (= 0.31) l_{F1}: length where $w < w_c$ w_c: maximum crack width for stress transfer f_c: compressive strength of concrete f_{ct}: tensile strength of concrete
Aggregate interlock V_{Agg} $\frac{V_{Agg}}{\sqrt{f_c} \cdot b} = \sin\beta_{AB} \cdot \frac{c_3 \cdot \bar{\delta}_A^{4/3}}{(c_2 \cdot \bar{\delta}_A + 0.8) \cdot \left(\frac{u_A}{d_F} \cdot \frac{c_2}{d_{dg}}\right)^{1.8+c_2\bar{\delta}_A}} \cdot \frac{l_2^{0.8+c_2\bar{\delta}_A} - l_1^{0.8+c_2\bar{\delta}_A}}{(l_2 \cdot l_1)^{0.8+c_2\bar{\delta}_A}}$ $- \cos\beta_{AB} \cdot \frac{c_4 \cdot \bar{\delta}_A^{7/3}}{(c_2 \cdot \bar{\delta}_A + 2) \cdot \left(\frac{u_A}{d_F} \cdot \frac{c_2}{d_{dg}}\right)^{3+c_2\bar{\delta}_A}} \cdot \frac{l_2^{2+c_2\bar{\delta}_A} - l_1^{2+c_2\bar{\delta}_A}}{(l_2 \cdot l_1)^{2+c_2\bar{\delta}_A}}$ $+ \cos\beta_{AB} \left[l_3 \cdot \left(1 - \frac{1}{1+c_1} \cdot \left(\frac{u_A \cdot l_3}{d_F \cdot w_c}\right)^{c_1}\right) - l_1 \cdot \left(1 - \frac{1}{1+c_1} \cdot \left(\frac{u_A \cdot l_1}{d_F \cdot w_c}\right)^{c_1}\right)\right] \cdot \frac{f_{ct}}{\sqrt{f_c}}$	Two-phase aggregate interlock model[14] with modified kinematics according to the study by Guidotti[15]	c_2, c_3, c_4: constants $\bar{\delta}_A = \delta_A / d_{dg}$ δ_A: crack sliding at point A d_{dg}: parameter to account for roughness f_c: compressive strength of concrete f_{ct}: tensile strength of concrete
Dowel action of the longitudinal reinforcement V_{Dow} $V_{Dow} = k_b \cdot f_{ct} \cdot n \cdot (b/n - d_b) \cdot 2 \cdot d_b$	[16]	k_b: strength reduction factor for bars under tension; 1.0 for continuously loaded members on the side of the tensile reinforcement[12] n: number of bars d_b: bar diameter f_{ct}: tensile strength of concrete
Contribution of the compression zone V_{Compr} $V_{Compr} = f_c \cdot b \cdot 2 \cdot c_m \cdot \tan\alpha_{cc}$ and $N_{compr} = \frac{M_F}{d_F - c/3} = f_c \cdot b \cdot 2 \cdot c_m \rightarrow c_m$	[12]	k_c: constant (= 0.5) h_f: uncracked height at x_F r_f: distance between point F and the support axis
Contribution of the inclined tensile reinforcement V_t $V_t = \varepsilon_s \cdot A_{sl} \cdot \tan(\alpha_t)$	[7]	ε_s: strains A_{sl}: area of the tensile reinforcement α_t: angle between the tensile reinforcement and the member axis